



## Polarization in Cells Containing Single-Ion Graft Copolymer Electrolytes

Patrick E. Trapa,<sup>a</sup> Allan B. Reyes, Raj Shekar Das Gupta,<sup>b,\*</sup> Anne M. Mayes,<sup>\*</sup> and Donald R. Sadoway<sup>\*,z</sup>

Department of Materials Science and Engineering, Massachusetts Institute of Technology, Cambridge, Massachusetts 02139-4307, USA

The single-ion conductor, BF<sub>3</sub>-incorporated poly[(oxyethylene)<sub>9</sub> methacrylate-*ran*-lithium methacrylate]-*graft*-poly(dimethyl siloxane), P(OEM-*r*-LiMA)-*g*-PDMS, was used as an electrolyte in cells containing a lithium anode and a thin-film vanadium oxide cathode. Cycle testing revealed an unanticipated high polarization which resulted in a significant drop in capacity compared to that of cells constructed with conventional salt-doped electrolytes produced by the addition of a lithium salt to an uncharged electrolyte poly(oxyethylene)<sub>9</sub> methacrylate-*graft*-polydimethyl siloxane. Impedance spectra obtained from a vanadium oxide symmetric cell fitted with a single-ion electrolyte showed a large resistance associated with the cathode/electrolyte interface. Further battery testing illustrated that the polarization remained even when lithium triflate was added to the single-ion electrolyte. In contrast, cells consisting of a lithium anode, single-ion electrolyte, and an alloying cathode showed no rise in polarization over what is found in similar cells constructed with a salt-doped electrolyte. These observations are consistent with the hypothesis that diffusion of lithium ions into the bulk vanadium oxide may be coulombically hindered by single-ion electrolytes.

© 2006 The Electrochemical Society. [DOI: 10.1149/1.2191188] All rights reserved.

Manuscript submitted August 15, 2005; revised manuscript received February 14, 2006. Available electronically April 13, 2006.

Conventional wisdom avers that electrolytes in which the lithium ion is the only mobile species, so-called single-ion conductors, have the capability of improving the performance of lithium batteries by reducing polarization at the electrodes. Detailed models suggest that mobile anions lead to concentration gradients that increase internal resistance and further reduce the capacity of the battery by creating depletion regions within composite electrodes.<sup>1</sup> Implicit in these simulations, however, is the assumption that single-ion electrolytes do not alter other key system parameters; most notably, the interface resistance between the electrolyte and cathode is assumed to be identical to that of a conventional cell with mobile charge carriers of both polarities.<sup>1</sup>

While in the literature there are many examples of conductivity studies of organic and hybrid organic/inorganic single-ion electrolytes, there are few reports of cycle testing such materials in a lithium battery construct. In 1996, Wan et al. investigated a blend of lithium methoxy oligo(oxyethylene) sulfate and poly(ethylene oxide).<sup>2</sup> The material had a room-temperature conductivity of  $1.2 \times 10^{-6}$  S/cm and performed well in lithium symmetric cells (dc conductivity  $> 1 \times 10^{-6}$  S/cm). However, when one of the lithium electrodes was replaced with an intercalation cathode of LiV<sub>3</sub>O<sub>8</sub>, high polarization was observed and thought to be associated with the electrolyte/cathode interface. Onishi et al. studied cells constructed with a polymer/aluminate single-ion electrolyte, a lithium anode, and a TiS<sub>2</sub> cathode.<sup>3</sup> These batteries similarly showed abnormally high polarization, which the authors of the article attributed solely to the low conductivity of the electrolyte, which they measured to be  $\sim 2 \times 10^{-7}$  S/cm. However, close inspection of the data reveals that over half of the polarization, in fact, arose from poor kinetics at, or ion transport across, the cathode/electrolyte interface. Recently, Riley et al. presented a detailed study of the cycling behavior of a composite single-ion conducting electrolyte comprising 0.5 M Li hectorite in propylene carbonate  $\sim 0.48$  g Li hectorite/g PC in batteries fitted with lithium anodes and composite LiCoO<sub>2</sub> cathodes.<sup>4</sup> They concluded that in these clay-based cells the values of the bulk electrolyte resistance as well as of the cathode charge-transfer resistance, cathode electronic/ionic resistance, and electrolyte/cathode surface-layer resistance were considerably higher than those for standard cells containing 1 M LiPF<sub>6</sub> in 1:1 w/w ethylene carbonate-

ethyl methyl carbonate. Clearly, even though the specific chemistries of the single-ion conducting electrolytes in these three studies varied considerably, in all cases when cells fitted with intercalation cathodes were cycled, an unanticipated increase in polarization was observed. In contrast, Onishi's work with nonintercalating (polymer) cathodes<sup>5</sup> suggests that single-ion electrolytes can be employed without increase in polarization under certain circumstances.

In the present study, we investigate the origins of the polarization in the presence of a single-ion electrolyte using poly[(oxyethylene)<sub>9</sub> methacrylate-*ran*-lithium methacrylate]-*graft*-polydimethyl siloxane, P(OEM-*r*-LiMA)-*g*-PDMS, complexed with BF<sub>3</sub> to promote ion dissociation and raise conductivity. Battery cycling data in conjunction with impedance measurements obtained with symmetric cells constructed with and without intercalating electrodes trace the site of the polarization to the interface between the single-ion electrolyte and an intercalation cathode. Further experimental evidence eliminates surface film growth and charge-transfer resistance as the cause, suggesting instead that lithium-ion diffusion into the bulk of the intercalation cathode may be hindered by the presence of bound, immobile negative charges in the electrolyte.

### Experimental

The synthesis and characterization of BF<sub>3</sub>-incorporated P(OEM-*r*-LiMA)-*g*-PDMS (75:14:11 wt %) has been previously described.<sup>6</sup> This material had a lithium-to-ethylene oxide ratio (Li/EO) of 1:8, which is too high a concentration of cations for optimum conductivity. The Li<sup>+</sup> concentration was diluted by the addition of uncharged poly(oxyethylene)<sub>9</sub> methacrylate-*graft*-polydimethyl siloxane (POEM-*g*-PDMS), prepared as reported previously.<sup>7</sup> The diluted systems were found to possess Li<sup>+</sup> transference numbers of approximately unity and a room-temperature conductivity of  $7 \times 10^{-6}$  S/cm at an optimum Li/EO ratio of 1:32. For comparison, charge carriers were added to POEM-*g*-PDMS through the addition of lithium triflate (Li/EO = 1:20), yielding a graft copolymer electrolyte (GCE) with a room-temperature conductivity of  $7.8 \times 10^{-6}$  S/cm. All of the above materials exhibited elastomeric mechanical properties due to their microphase-separated morphology.<sup>7-11</sup>

To study the single-ion electrolyte's performance in a solid-state battery, BF<sub>3</sub>-incorporated P(OEM-*r*-LiMA)-*g*-PDMS (Li/EO = 1:24,  $\sigma \sim 5 \times 10^{-6}$  S/cm) was blended with 10% poly(ethylene glycol) dimethyl ether (PEGDME,  $M_w \approx 500$ , Aldrich) and placed in test cells fitted with a thin-film cathode of vanadium oxide on aluminum foil and an anode of lithium. The cathode films were prepared by depositing vanadium oxide onto an aluminum foil

\* Electrochemical Society Active Member.

<sup>a</sup> Present address: ElectroVaya, Mississauga, Ontario, Canada L5J 1K9.

<sup>b</sup> Present address: Department of Materials Science and Metallurgy, University of Cambridge, Cambridge CB2 3QZ, U.K.

<sup>z</sup> E-mail: dsadoway@mit.edu

**Table I. Compositions of the electrolytes used in the Li/Li<sup>+</sup>/VO<sub>x</sub> cells subjected to cycle testing, the results of which are reported in Fig. 5.**

	GCE (undoped) (g)	1:8 BF <sub>3</sub> - SIGCE (g)	PEGDME (g)	LiTr (g)	Li <sup>+</sup> from salt (%)
Sample 1	0.20	0.05	0.025	0.02	61
Sample 2	0.15	0.1	0.025	0.002	7.3
Sample 3	0.14	0.1	0.024	0.0002	0.8
Sample 4	0.14	0.1	0.024	None	0
Sample 5	0.15	None	0.015	0.024	100

substrate (thickness  $\sim 20 \mu\text{m}$ ) by ion-assisted, electron-beam evaporation of vanadium metal at  $320^\circ\text{C}$  in a controlled oxygen environment. The films were subsequently annealed in air at  $250^\circ\text{C}$  for 2 h. Oxide film thicknesses were determined to be  $\sim 0.2 \mu\text{m}$  as measured by profilometry. Broad peaks in the X-ray diffraction (XRD) patterns taken with a rotating anode and Cu  $K\alpha$  radiation (Rigaku RTP500RC) revealed the oxide films to be partially crystalline and comprised of multiple phases. Some peaks were identified as those associated with  $\text{V}_2\text{O}_3$ ; others could not be matched to any known member of the V–O system. By Auger electron spectroscopy the vanadium concentration of the oxide films was measured to be  $39 \pm 2\%$  on an atomic basis, which puts their stoichiometry between  $\text{V}_2\text{O}_3$  and  $\text{V}_2\text{O}_4$ ; accordingly, we refer to the films simply as  $\text{VO}_x$ , where  $1.5 < x < 2$ . Electrolyte films measuring 45 and  $90 \mu\text{m}$  in thickness were prepared by solution casting from a 1:1 mixture of anhydrous tetrahydrofuran (THF) (Aldrich) and methanol (Aldrich) directly onto the  $\text{VO}_x$  film in an argon-filled glove box. The electrolyte/cathode construct was then dried under vacuum for 2 h before final cell assembly.

Cycle testing was conducted at  $23^\circ\text{C}$  with a MACCOR series 4000 automated test system. Voltage limits were set at 3.9 and 1.5 V. Discharge and charge rates were identical and fixed at  $12.7 \mu\text{A}/\text{cm}^2$ , which was approximately a C/1.5 rate. Each charge and discharge was followed by a 1 min rest period during which time the open-circuit voltage (OCV) was monitored. In order to gain information about the rate-limiting mechanism, the above batteries were subjected to ac impedance testing using a 10-mV ripple around their respective OCVs. Subsequent cells were similarly constructed and cycled between 2.1 and 3.9 V at a rate of  $13 \mu\text{A}/\text{cm}^2$  using a Solartron 1286 potentiostat. The electrolyte compositions (Li/EO  $\approx 1:17$ ) of these cells are given in Table I. In addition, single-ion GCEs (SIGCEs) and conventional salt-doped GCEs were incorporated into cells constructed with alloying cathodes made of pure gold. These batteries were tested with a Solartron 1286 between 0.15 and 1.8 V at  $13 \mu\text{A}/\text{cm}^2$ . The initial discharge, however, began at the OCV, which is  $\sim 3.4$  V for these cells.

In an attempt to eliminate specific, unfavorable electrolyte/electrode interfaces, cells fitted with a bilayer electrolyte consisting of the GCE and the SIGCE were constructed. By design, in some cells the GCE contacted the lithium anode while the SIGCE contacted the  $\text{VO}_x$  cathode, i.e., Li/GCE/SIGCE/ $\text{VO}_x$ ; in others, the complementary orientation was chosen, i.e., Li/SIGCE/GCE/( $\text{VO}_x$  or Au). The polymer electrolyte contained 10% PEGDME, and the lithium concentration was held constant at Li/EO  $\approx 1:17$ . Cycle testing was conducted with a Solartron 1286 at a current rate of  $13 \mu\text{A}/\text{cm}^2$  between 2.1 and 3.9 V.

The impedance spectra of symmetric cells constructed with pairs of  $\text{VO}_x$  electrodes and pairs of lithium electrodes were measured in an effort to isolate the contributions of the different types of electrode/electrolyte interfaces. The interfacial resistance can be derived from the diameter of the second semicircle in the Cole–Cole plot.

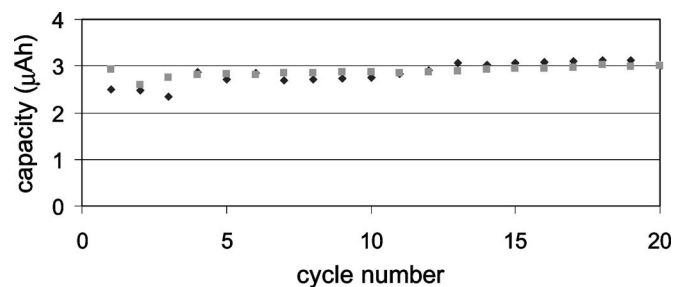
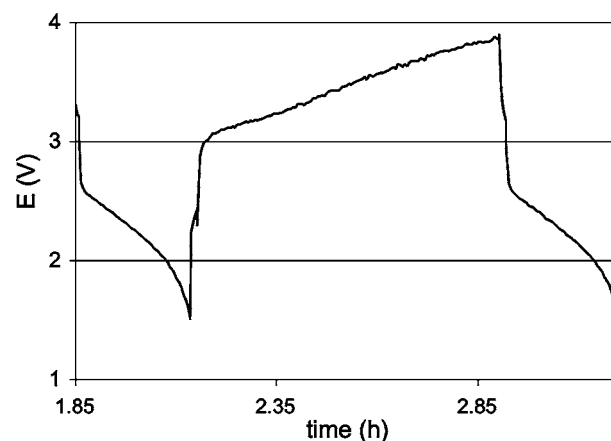


**Figure 1.** Cycle test data for two cells composed of a lithium anode,  $\text{VO}_x$  cathode, and a  $\text{BF}_3$ -incorporated P(OEM-*r*-PLiMA)-*g*-PDMS electrolyte (Li/EO = 1:24).  $i_c = i_d = 12.7 \mu\text{A}/\text{cm}^2$ ,  $3.9 \text{ V} > V > 2.1 \text{ V}$ .

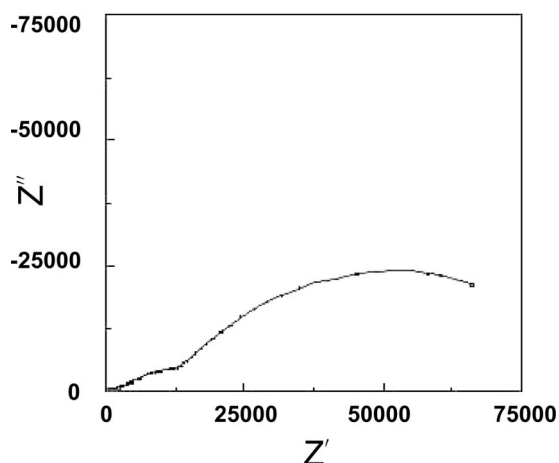
## Results and Discussion

Figure 1 shows cycling data for batteries prepared using the  $\text{BF}_3$ -incorporated SIGCE. While the cells exhibited very little capacity fade, the absolute magnitude of the capacity was found to be roughly 60% less than that expected based upon tests conducted with otherwise identical cells fitted with a conventional salt-doped electrolyte. The charge and discharge curves clearly indicate a large polarization (Fig. 2), as evidenced by the near-vertical slope in the voltage trace at the beginning of the charge and discharge steps. An impedance spectrum obtained after 20 cycles revealed a large incomplete semicircle at the low-frequency (right) side of the Cole–Cole plot (Fig. 3), indicative of a highly resistive interfacial process. The magnitude of the associated resistance is large enough to account for the polarization drops shown in Fig. 2. Impedance data taken on symmetric cells composed of pairs of  $\text{VO}_x$  electrodes ( $\text{VO}_x/\text{SIGCE}/\text{VO}_x$ ) and pairs of Li electrodes (Li/SIGCE/Li) are shown in Fig. 4. The diameter of the first semicircle at the high-frequency (left) side of the Cole–Cole plot corresponds to the resistance of the electrolyte. The Li symmetric cell showed a higher electrolyte resistance than the  $\text{VO}_x$  counterpart because the polymer layer was thicker in the Li cell. More importantly, however, the  $\text{VO}_x$  cell exhibited a large interface resistance as evidenced by the diameter of the second, incomplete semicircle. This suggests that the polarization apparent in Fig. 2 is associated with a process involving heterogeneous kinetics either at an interface within the  $\text{VO}_x$  cathode or at the cathode/electrolyte interface.

The polarization at the cathode may be explained by one of the following: (i) slow transport of  $\text{Li}^+$  to the surface of the electrode due to either (a) the presence of a surface film or (b) low conductivity of the electrolyte, (ii) slow electron transfer at the electrode/electrolyte interface, or (iii) slow diffusion of the  $\text{Li}^+$  away from the



**Figure 2.** The voltage trace of the cell described in Fig. 1. Depicted are the 3rd discharge, 3rd charge, and 4th discharge.



**Figure 3.** The impedance spectrum of the cell described in Fig. 1 after 20 charge–discharge cycles.

surface of the electrode and into the bulk ceramic. Explanations 1a and b seem unlikely. Passivating films do not form on  $\text{VO}_x$  in contact with the GCE, and the presence of  $\text{BF}_3$  moieties complexed with carboxylate ions along the methacrylate backbone of the SIGCE is not expected to affect the chemical reactivity with  $\text{VO}_x$ . Furthermore, to check whether unreacted  $\text{BF}_3$  possibly entrained in the SIGCE could be the source of a reactant with the potential to form a resistive film, samples of  $\text{VO}_x$  were immersed in a solution of THF containing  $\text{BF}_3$  at a concentration exceeding that used in the synthesis of the SIGCE. No evidence of the formation of a resistive film was apparent from cycle tests performed on cells in which these substrates served as the cathode. Furthermore,  $\text{BF}_3$  was added to the conventional salt-doped electrolyte at a concentration exceeding that used in the synthesis of the SIGCE. Samples of  $\text{VO}_x$  were exposed to this. As was the case above, no increase in polarization was observed. Regarding the conductivity of the electrolyte, values for this material<sup>6</sup> are too high to account for the resistance observed in Fig. 2.

In light of the data presented up to this point, it is not possible to distinguish between mechanisms 2 and 3. The remaining experiments in this study were designed to do so.

Graft copolymer electrolytes incorporating both bound and mobile anions were placed in cells and cycled. Figure 5 shows the seventh discharge of cells constructed with a  $\text{VO}_x$  cathode, lithium

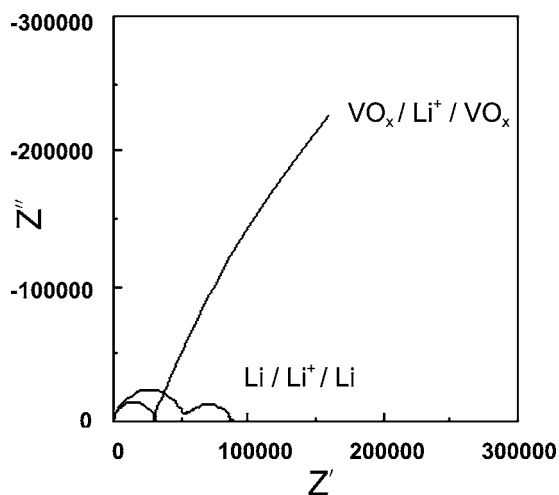


**Figure 4.** Impedance spectra of lithium and  $\text{VO}_x$  symmetric cells containing  $\text{BF}_3$ -incorporated SIGCE (Li/EO = 1:24).

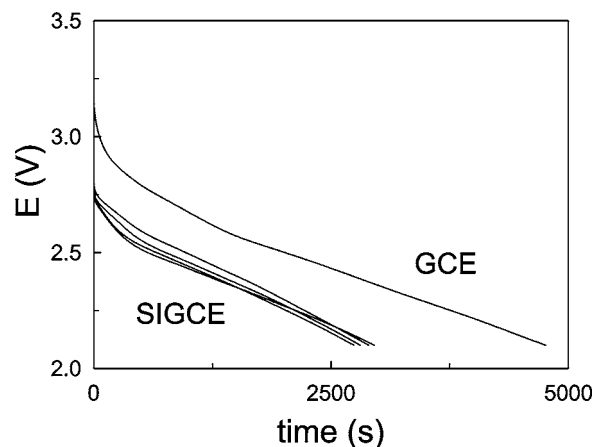


**Figure 5.** The 7th discharge of Li/Li<sup>+</sup>/VO<sub>x</sub> cells with the electrolyte compositions defined in Table I.  $i_c = i_d = 13 \mu\text{A}/\text{cm}^2$ ,  $3.9 \text{ V} > V > 2.1 \text{ V}$ .

anode, and the SIGCE doped with various amounts of LiTr as specified in Table I. All of the cells containing the SIGCE behaved similarly, regardless of how much lithium triflate (LiTr) was present, and as a group exhibited worse performance than the cell containing a conventional salt-doped GCE with no immobile anions. This is an indication that the polarization in the SIGCE-based electrolytes does not originate strictly from a resistance to charge transfer because one would expect the presence of added salt with its mobile anions to mitigate such an effect.

In a further attempt to understand the origin of the polarization, batteries were constructed with bilayer electrolytes such that a conventional salt-doped GCE contacted the  $\text{VO}_x$  cathode and a SIGCE contacted the lithium metal anode, i.e., Li/SIGCE/GCE/ $\text{VO}_x$ . Cycle testing showed the performance of such cells to be superior initially to that of an identical cell fitted with the SIGCE but still far inferior to cells incorporating a conventional salt-doped GCE. However, after a few cycles the performance of the cell containing the bilayer electrolyte degraded to that of a cell constructed with the SIGCE alone (presumably because the polymer layers mixed). The behavior can be explained by the Donnan equilibrium<sup>12-15</sup> and would place the site of the attendant kinetic bottleneck at the interface between the two polymer layers. This, then, points to mechanism 3 as the likely cause of the observed rise in polarization. By the introduction of the salt-doped GCE between the cathode and the SIGCE, the site of retarded  $\text{Li}^+$  diffusion is shifted to the SIGCE/GCE interface.

As a final experiment, the performances of single-ion and salt-doped electrolytes were compared in cells constructed with lithium anodes and gold cathodes. Cycle testing results are shown in Fig. 6. Here, the SIGCE and the conventional salt-doped GCE were found to behave similarly. The characteristic features in the discharge curve occur at the same potentials for both systems, indicating that the cells experience an equivalent level of polarization. Unlike in cells with intercalation cathodes, where  $\text{Li}^+$  inserts and remains a cation and the charge compensation occurs on the transition metal and oxygen,<sup>16,17</sup> in cells with gold cathodes  $\text{Li}^+$  is reduced to neutral metallic  $\text{Li}^0$ , which alloys with the gold. The authors speculate that the polarization found in the intercalation cathodes (in this study and in the examples cited from the literature<sup>2-4</sup>) is the result of coulombic attraction between the  $\text{Li}^+$  attempting to intercalate and the bound anion in the electrolyte, which is free to approach the positively charged cathode thanks to the segmental mobility of the polymer backbone. The attractive electrostatic force between the bound anion and the  $\text{Li}^+$  attempting to intercalate would thus represent an additional activation barrier to the ingress of lithium at the electrode/electrolyte interface and would manifest itself in the form of polarization, i.e., an activation overpotential. We further postulate that the bound anion is near enough to the surface of the cathode that even

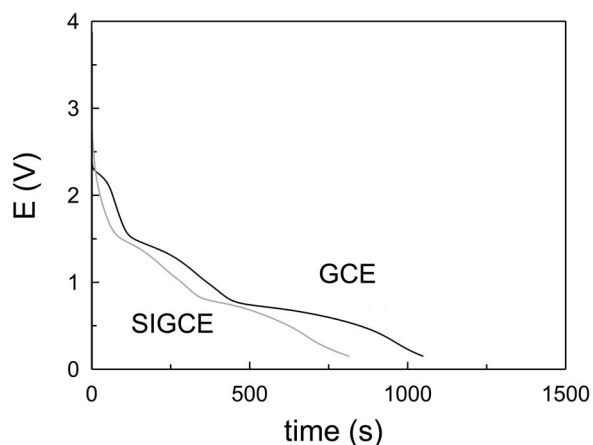


**Figure 6.** First discharge of cells fitted with a lithium anode, gold cathode, and a GCE (Li/EO  $\approx$  1:20) or BF<sub>3</sub>-incorporated SIGCE.  $i_c = i_d = 13 \mu\text{A}/\text{cm}^2$ ,  $V > 0.15 \text{ V}$ .

with the addition of salt the immobile charge cannot be effectively screened. The bilayer results vividly show that even when the bound anions are pushed away from the cathode by a distance equal to the thickness of the GCE layer, high polarization is still measured. In contrast, electrodes at which the reaction is either alloying or plating are not expected to exhibit excessive polarization because in these reactions, lithium converts to neutral valence and is no longer susceptible to coulombic hindrance by the immobile anions. This explains also why single-ion electrolytes perform well in lithium symmetric cells. As for the importance of segmental motion in enabling close approach of the immobile anions to the cathode, single-ion conductors such as LiPON are immune to the polarization effect seen in the cells described in the present study because below the glass-transition temperature the anions in an oxide glass are frozen in place and therefore cannot migrate to the cathode/electrolyte interface.<sup>18</sup>

### Conclusions

We have shown that the use of a single-ion polymer electrolyte, BF<sub>3</sub>-incorporated P(OEM-*r*-LiMA)-*g*-PDMS, in Li/Li<sup>+</sup>/VO<sub>x</sub> cells

leads to unanticipated polarization at the cathode. This is consistent with the observations of previous studies involving other single-ion electrolytes.<sup>2-4</sup> Impedance measurements and cycle testing of cells consisting of various combinations of electrolyte (single-ion or salt-doped) and cathode (intercalating or alloying) lead us to speculate that electrostatic attraction between the Li<sup>+</sup> attempting to intercalate into the cathode and the bound anion in the electrolyte gives rise to the observed polarization. Our results suggest that the putative superior performance of batteries with single-ion electrolytes may rest upon an incomplete accounting of the operative elementary processes.

### Acknowledgments

Support for this research by the U.S. Office of Naval Research under awards N00014-99-1-0561, N00014-99-1-0565, and N00014-02-1-0226 is gratefully acknowledged.

Massachusetts Institute of Technology assisted in meeting the publication costs of this article.

### References

1. M. Doyle, T. F. Fuller, and J. Newman, *Electrochim. Acta*, **39**, 2073 (1994).
2. H. Chen, Z. Deng, Y. Zheng, W. Xu, and G. Wan, *J. Macromol. Sci., Pure Appl. Chem.*, **A33**, 1273 (1996).
3. K. Onishi, M. Matsumoto, and K. Shigehara, *J. Power Sources*, **92**, 120 (2001).
4. M. W. Riley, P. S. Fedkiw, and S. A. Khan, *J. Electrochem. Soc.*, **150**, A933 (2003).
5. K. Onishi, M. Matsumoto, and K. Shigehara, *J. Electrochem. Soc.*, **147**, 2039 (2000).
6. P. E. Trapa, M. H. Acar, D. R. Sadoway, and A. M. Mayes, *J. Electrochem. Soc.*, **152**, A2281 (2005).
7. P. E. Trapa, Y.-Y. Won, S. C. Mui, E. A. Olivetti, B. Huang, D. R. Sadoway, A. M. Mayes, and S. Dallek, *J. Electrochem. Soc.*, **152**, A1 (2005).
8. F. S. Bates, *Macromolecules*, **17**, 2607 (1984).
9. F. S. Bates, H. E. Bair, and M. A. Hartney, *Macromolecules*, **17**, 1987 (1984).
10. P. E. Trapa, B. Huang, Y.-Y. Won, D. R. Sadoway, and A. M. Mayes, *Electrochem. Solid-State Lett.*, **5**, A85 (2002).
11. P. P. Soo, B. Huang, Y.-I. Jang, Y.-M. Chiang, D. R. Sadoway, and A. M. Mayes, *J. Electrochem. Soc.*, **146**, 32 (1999).
12. M. D. Afonso and M. N. de Pinho, *J. Membr. Sci.*, **179**, 137 (2000).
13. F. G. Donnan, *Z. Elektrochem. Angew. Phys. Chem.*, **17**, 572 (1911).
14. F. G. Donnan, *Chem. Rev. (Washington, D.C.)*, **1**, 73 (1924).
15. F. G. Donnan, *Z. Phys. Chem. Abt. A*, **168**, 369 (1934).
16. M. K. Aydinol, A. F. Kohan, G. Ceder, K. Cho, and J. Joannopoulos, *Phys. Rev. B*, **56**, 1354 (1997).
17. G. Ceder, Y.-M. Chiang, D. R. Sadoway, M. K. Aydinol, Y.-I. Jang, and B. Huang, *Nature (London)*, **392**, 694 (1998).
18. X. Yu, J. B. Bates, G. E. Jellison, Jr., F. X. Hart, *J. Electrochem. Soc.*, **144**, 524 (1997).